Solar Phys (2007) 240: 271–281
DOI 10.1007/s11207-006-0337-5

Spatial Characterization of a Flare Using Radio Observations and Magnetic Field Topology

G. Cristiani · G. Martinez · C.H. Mandrini · C.G. Giménez De Castro · C.W. Da Silva · M.G. Rovira · P. Kaufmann

Received: 12 October 2006 / Accepted: 13 December 2006 /
Published online: 8 March 2007

Abstract Using magnetograms, EUV and Hα images, Owens Valley Solar Array microwave observations, and 212-GHz flux density derived from the Solar Submillimeter Telescope data, we determine the spatial characteristics of the 1B/M6.9 flare that occurred on November 28, 2001, starting at 16:26 UT in active region (AR) NOAA 9715. This flare is associated with a chromospheric mass ejection or surge observed at 16:42 UT in the Hα images. We compute the coronal magnetic field under the linear force-free field assumption, constrained by the photospheric data of the Michelson Doppler Imager and loops observed by the Extreme Ultraviolet Imaging Telescope. The analysis of the magnetic field connectivity allows us to conclude that magnetic field reconnection between two different coronal/chromospheric sets of arches was at the origin of the flare and surge, respectively. The optically thick microwave spectrum at peak time shows a shape compatible with the emission from two different sites. Fitting gyrosynchrotron emission to the observed spectrum, we derive parameters for each source.

Keywords Flares · Relation to magnetic field · Magnetic reconnection · Observational signatures · Radio burst · Association with flares · Radio burst · Dynamic spectrum · Surges

Electronic Supplementary Material The online version of this article (http://dx.doi.org/10.1007/s11207-006-0337-5) contains supplementary material, which is available to authorized users.

G. Cristiani (✉) · G. Martinez · C.H. Mandrini · M.G. Rovira
Instituto de Astronomía y Física del Espacio, CONICET-UBA, CC. 67, Suc. 28,
1428 Buenos Aires, Argentina
e-mail: gcristiani@iafe.uba.ar

C.G. Giménez De Castro · C.W. Da Silva · P. Kaufmann
Centro de Radio Astronomia e Astrofísica Mackenzie, Universidade Presbiteriana Mackenzie,
Sao Paulo, Brazil

P. Kaufmann
CCS, Universidade Estadual de Campinas, Campinas, SP, Brazil

1. Introduction

Radio bursts observed at frequencies above a few GHz, are mainly originated by gyroemission of mildly relativistic or relativistic non-thermal electrons. Since gyroemission is sensitive to the magnetic field of the medium, radio observations may give clues about the flaring magnetic configuration. The opposite is also true: Once the magnetic field configuration is known, we may be able to explain the characteristic of the burst (Bastian, Benz, and Gary, 1998). Moreover, it is widely accepted that sudden changes in the magnetic topology (also known as magnetic reconnection) release energy that ultimately accelerates particles through processes yet to be fully understood. Therefore, the simultaneous analysis of the magnetic topology and radio observations may give insights into the characteristics of the emitting sources.

In this work we extend a previous analysis (Cristiani *et al.*, 2005, hereafter Paper I) of the 1B/M6.9 flare that occurred on November 28, 2001, in NOAA active region (AR) 9715, and the chromospheric ejection that followed it. In Paper I, the analysis of the magnetic field evolution and Hα morphology identified the interaction between emergent flux and the pre-existing magnetic field as the origin of the energy release responsible for the radio emission enhancement and Hα brightenings. In the present work, a detailed quantitative magnetic field reconstruction allows us to conclude that magnetic reconnection occurred in two different loop systems of low height. We add observations from Owens Valley Solar Array (OVSA; Hurford, Read, and Zirin, 1984) to our previous analysis. The microwave spectrum during the impulsive phase shows two peaks at different frequencies, unlike the classical gyrosynchrotron emission. Therefore, the gyrosynchrotron emissions of two distinct and separate homogeneous sources were computed by using the theory developed by Ramaty *et al.* (1994) and Ramaty (1969) and their composition was fitted to the observed radio spectrum at peak time.

In Section 2, we summarize the photospheric and chromospheric observations, already discussed in Paper I, that are relevant to this study. In Section 3, we compute the coronal magnetic field model and discuss its connectivity. We determine the radio spectrum during the impulsive phase of the flare and we compute the parameters of the emitting electrons, assuming the composition of the gyrosynchrotron emission from two different sites, in Section 4. In the final section, we conclude on the mechanisms that originated the radio emission, and we discuss the results of Paper I in the context of the magnetic field model obtained in Section 3.

2. Summary of the Observations

Figure 1a shows the line-of-sight magnetic field, as observed by the Michelson Doppler Imager (MDI; Scherrer *et al.*, 1995), at the time closest to the 1B/M6.9 flare. AR 9715, which appeared at the eastern solar limb as mainly bipolar (polarities 1 and 2 in Figure 1a), was formed by several bipoles at the time of the flare. We could identify at least two episodes of flux emergence (polarities 5 and 6, and 7 and 8) from November 26 to November 28, which are described in Paper I. The polarities in Figure 1a are numbered as in Paper I, except that here we have added the label "r1" to point to a small positive flux concentration, probably part of polarity 1 when it disintegrated during its decay phase. For better understanding of the AR evolution, we accompany this paper with an MDI movie covering from early November 26 to two days after the flare (`mdi-evol-26-30nov.mpeg`). In this movie the magnetic data have been saturated as in Figure 1.

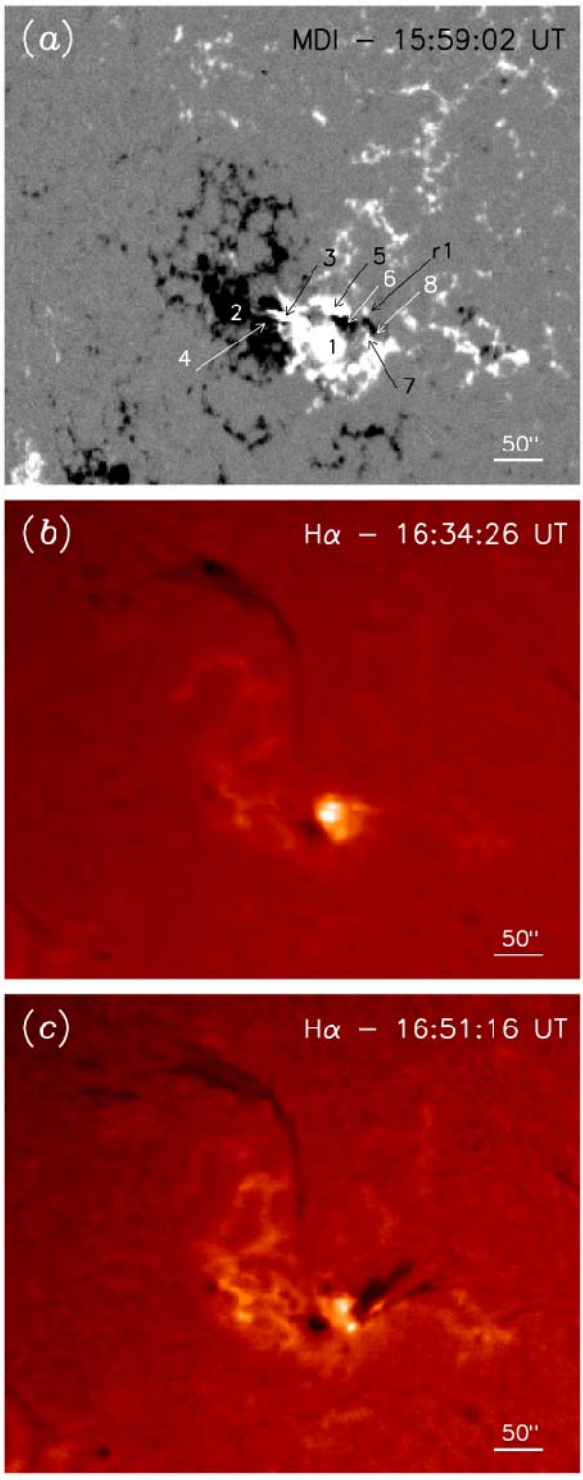

Figure 1 The photospheric and chromospheric data registered by MDI and HASTA during November 28, 2001. (a) MDI magnetogram closest in time to the flare. The area covered by the panel is 300 × 250 pixels (1 pixel side ≈ 1.98″). The magnetic field is saturated above (below) 200 G (−200 G). The numbers correspond to the different polarities mentioned in the text. (b) Flare kernels during maximum in Hα. (c) Dark chromospheric material ejected toward the North-West. The area covered by panels (b) and (c) is 284 × 236 pixels (1 pixel side ≈ 2.07″). The field of view is the same in the three panels.

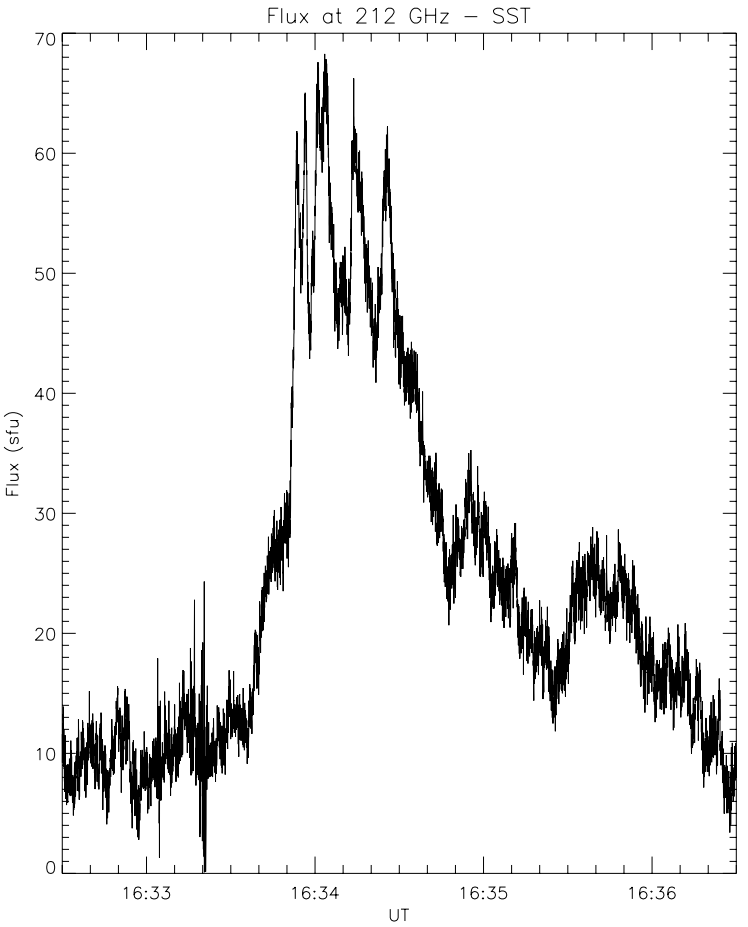

Figure 2 The SST 212-GHz flux density during the flare.

The 1B flare had its maximum in Hα at 16:34 UT, and it appeared as two intense kernels lying on polarities 6 and 1 (North) (see Figure 1b). Two brightenings were observed all along the Hα Solar Telescope for Argentina (HASTA; Fernández Borda *et al.*, 2002) observations (from 11:12 UT to 21:58 UT) at the same location. As the flare decayed, the Hα emission shifted toward the West (see Figure 1c).

Starting at around 16:42 UT and until 17:04 UT, dark chromospheric material ejected (a surge) in the North-West direction was observed in HASTA images. By backward extrapolation we estimated the starting time of the surge as ≈16:34 UT (see Paper I), so close in time to flare maximum in Hα. At the North of the active region a long filament can be seen in Hα images; it also appears as a dark gap in the EUV image shown in Figure 3. This filament was seen to change its shape and move during the flare (compare Figures 1b and c).

Microwave observations in the range 1 – 18 GHz with 8 s time resolution were recorded by OVSA with imaging capabilities for 10 to 12 frequencies. Observations at 212 and 405 GHz were obtained with the Solar Submillimeter Telescope (SST; Kaufmann *et al.*, 2000). We have revised the 212-GHz flux obtained in Paper I using a numerical algorithm

adapted from a multibeam technique (Costa *et al.*, 1995) that takes into account the real beam shapes instead of Gaussian beams. Beam shapes were determined at 212 GHz with radial raster solar scans and a tomographic inversion method (Costa *et al.*, 2002), while at 405 GHz a direct measurement of the beam was carried on by means of a beacon. This implementation of the multibeam technique assumes that source sizes are much smaller than beam sizes and works to find numerically the source position that minimizes the difference between the expected and the observed ratios of antenna temperatures at 212 GHz. Once the source position is determined, the antenna temperature is corrected by the offset of the main beam with respect to the source. This procedure gives a correct flux density. By assuming the same source position at 405 GHz a correction for the offset at 405 GHz is also made. The resulting new flux densities are quantitatively different from the ones shown in Paper I, but the time profiles are similar. Details of this numerical method will be published elsewhere. The comparison between radio flux time profiles and Hα lightcurves showed a notable agreement (see Figure 4 in Paper I), with a delay of less than 12 s, the time resolution of the Hα telescope. At 405 GHz, significant radio emission was not observed above the noise level during the impulsive flare phase; the flux density standard deviation (30 sfu) was then adopted in this temporal range as an upper bound for the emission. At 212 GHz, a considerable enhancement of emission and a very structured time profile was observed, exhibiting five peaks in the 1 – 5 s range (see Figure 2). When comparing the source location of each peak, we find a very low dispersion of the order of 10″ (see Paper I). Microwave emission (OVSA) shows an impulsive peak with maximum flux density values that range from 250 sfu (1.2 GHz) to 1800 sfu (15.6 GHz).

3. Coronal Magnetic Field Model

Coronal observations, like those provided by the Extreme Ultraviolet Imaging Telescope (SOHO/EIT; Delaboudinière *et al.*, 1995), let us identify the magnetic loops that are significantly heated and, therefore, are denser and hotter than the surrounding ones. However, to understand the origin of the emission described in the previous sections we need additional information about the coronal connectivities and their possible changes. This can be provided by a model of the coronal field.

We compute the coronal magnetic field under the linear (or constant α) force-free field assumption ($\vec{\nabla} \times \vec{B} = \alpha \vec{B}$), using a fast Fourier transform method, as proposed by Alissandrakis (1981). Our model takes into account the transformation of coordinates from the AR location to disk center (see Mandrini *et al.*, 1996; Démoulin *et al.*, 1997).

We take, as boundary condition for the model, the MDI magnetogram closest in time to the flare (see Figure 1a). The value of the free parameter α is determined to best fit the EIT loops observed in 195 Å at a given time (Figure 3, top). Since during the flare EIT data were saturated and it was not possible to distinguish loops, we took the non-saturated EIT image closest in time to the MDI magnetic map (≈15:36 UT) for this fitting. The value of α is computed through an iterative process. First, we compute the coronal field assuming a given value for α; then, we compute the mean distance between the observed EIT loops and the closest computed field lines. Finally, through successive steps we select the value of α that gives the best global fit (*i.e.*, smallest mean distance), as discussed in Green *et al.* (2002). We have found that two different values of α are needed to best match EIT loops; the largest in absolute value ($\alpha = -0.09$ Mm^{-1}) gives a better agreement to the loops at the North of the AR, while the lowest ($\alpha = -0.06$ Mm^{-1}) fits better the loops at the South. In principle, this is logical since it is expected that the magnetic shear be high in regions where filaments are present, as is the case of the North-Eastern portion of AR 9715 (see Figures 1b and c).

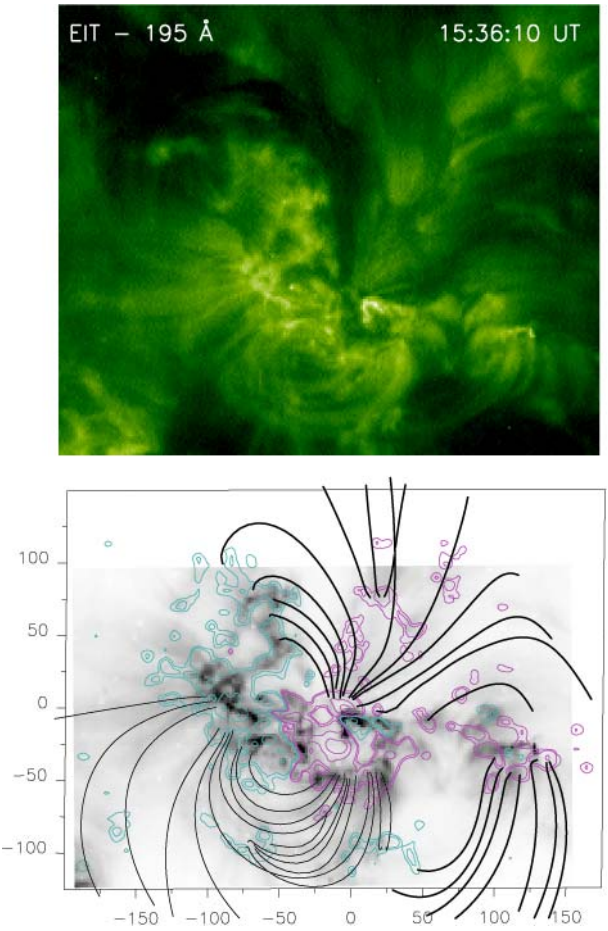

Figure 3 EIT 195 Å observation and magnetic field model. The top panel shows an EIT image at 15:36 UT. Some EIT loops are clearly seen at this time in the absence of flaring. The area covered by the panel is 224×187 pixels (1 pixel side $\sim 2.62''$). The field of view is the same as in Figure 1. Part of the same image is shown in the bottom panel (in reverse intensity) together with MDI isocontours (± 50, 100, 500, 1000 G); positive/negative values are drawn with pink/blue thin lines. Some magnetic field lines following the shape of EIT loops have been superimposed (the thin black lines have been computed using $\alpha = -0.06$ Mm^{-1} and the thick ones using $\alpha = -0.09$ Mm^{-1}). The figure shows the connectivity of field lines overlaying the neutral line along which the filament lies (compare to Figures 1b and c). In the bottom panel, both axes are measured in Mm.

3.1. Magnetic Connectivity and the Observed Events

Once the coronal model is determined, we analyze the magnetic connectivity in the neighborhood of the flare kernels. The set of field lines linking the polarities 5 – 6, belonging to one of the new emerging bipoles to the West (see Figure 4 and `mdi-evol-26-30nov.mpeg`), could interact with field lines starting from the AR pre-existing field (dark blue lines anchored in polarity 1 in Figure 4, top). This interaction could have started very early on November 28, as shown by the presence of the two brightenings in the first Hα images obtained by HASTA on that day. As 5 – 6 continued to emerge more quickly, this interaction, via magnetic reconnection, could have given place to the impulsive flare.

As a result of the just described magnetic reconnection processes, energy could have been released at very low atmospheric heights. In principle, the interaction of the bipole formed by polarities 5 and 6 with the surrounding AR field gives rise to two very intense, impulsive, and localized flare kernels. These lie over polarities 6 and 1, and we notice that part of the Hα kernel to the North overlays polarity 5 (with our co-alignment error between HASTA and MDI staying within ± 1 HASTA pixel). In this reconnection process, the released energy goes into low and dense loops and very extended and steep field lines starting from 5 (see

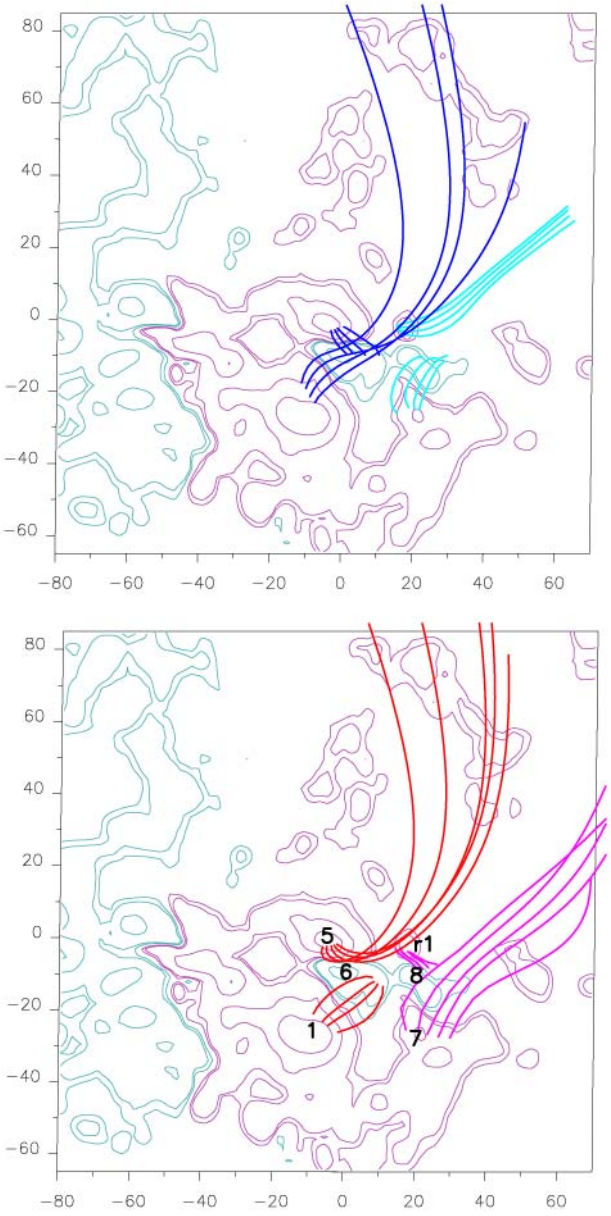

Figure 4 Magnetic field model of AR 9715. The top panel represents the magnetic connectivities before the flare. We have computed magnetic field lines anchored in the polarities (5 – 6, thick dark blue lines, and 7 – 8, thick light blue lines) belonging to the two emerging bipoles located at the West of the AR. As these bipoles emerge they interact, via magnetic reconnection, with the pre-existing magnetic field (field lines starting from polarity 1, dark blue lines, and r1, light blue lines; see text) that connects to regions outside of the studied AR. The bottom panel represents the connectivities after magnetic reconnection has occurred: One set of reconnected field lines joins now polarities 1 to 6 (thick red lines) and r1 to 8 (thick pink lines); the other two sets are anchored in 5 (thick red lines) and 7 (thick pink lines) and extend out of the AR. Notice that the shape of these very extended field lines agrees with that of the Hα surge. The isocontours of the field are ±50, 100, 500, 1000 G; positive/negative values are drawn with thin pink/blue lines. Polarities are numbered in the bottom figure.

the thick red lines in Figure 4, bottom panel). We do not observe any ejected chromospheric material along these field lines.

Another interaction, via magnetic reconnection, can be identified between the bipole formed by polarities 7 and 8 and the pre-existing magnetic field of polarity 1 to the West ("r1" in Figure 4). As the flare evolved, we observe that the Hα kernels extended toward the West, overlaying polarities 7, 8, and partially "r1" (taking into account co-alignment errors). A surge event is observed in HASTA images starting from polarity 7 at ≈16:42 UT. The

shape of the very extended field lines anchored in 7 (thick pink lines in Figure 4, bottom) agrees with that of the dark chromospheric material. The extension of the Hα kernels toward the West would indicate that the energy released in this reconnection process could go into very low, probably chromospheric, and dense loops linking 8 to "r1" and, at the same time, would gives rise to the observed surge.

4. Radio Spectrum

Figure 5 shows the radio spectrum at peak time with its two maxima: one around 14 – 16.5 GHz and the second around 8 – 12 GHz. These two maxima could be produced within the same magnetic loop having different field intensity at the top and footpoints. This would mean that the emitting source is inhomogeneous but, because it is the same magnetic structure, we would expect a continuous magnetic field intensity variation from top to bottom. The effect produced by such a continuous variation is a flattening of the optically thick part of the spectrum (Klein, Trottet, and Magun, 1986; Lee, Gary, and Zirin, 1994; Simões and Costa, 2006). As will be shown below, the optically thick part of our spectrum is very well fitted by the gyroemission of a homogeneous source. Therefore, since the analysis of the magnetic topology shows that reconnection could have taken place in two different and separate sites, we decided to model the gyrosynchrotron emission as the composition of two homogeneous sources, where electrons were accelerated and then radiated spiraling down through the magnetic arches. We envisage two different scenarios: (1) sources do not overlap along the line of sight (Model 1) and (2) sources partially overlap (Model 2). If sources overlap along the line of sight, only the outermost source emission can be seen from Earth in the optically thick regime, while the addition of both emissions forms the optically thin regime. If sources do not overlap, then the entire emission is composed by the sum of those coming from both sources. Radio images would be useful to discriminate between

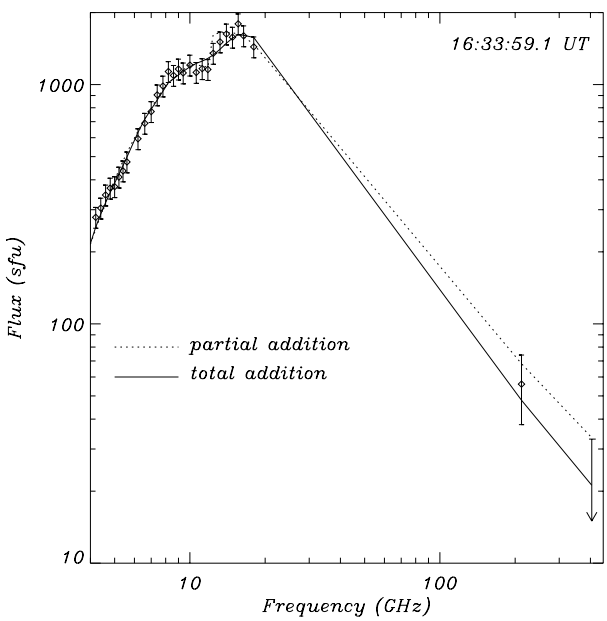

Figure 5 Instantaneous radio spectrum during the maximum of emission (16:33:59 – 16:34:08 UT). The diamonds correspond to the observed data, the continuous line to Model 1, and the dotted line to Model 2. The parameter values that provide the best fit to the data are shown in Table 1.

Table 1 Derived parameters from microwave spectral fits.

Parameter	Model (1)		Model (2)		Units
	Source 1	Source 2	Source 1	Source 2	
δ	3.1	3.5	2.95	3.45	
N_e	1.6	7.2	2.1	6.0	$\times 10^9$ cm^{-3}
E_0	0.027	0.025	0.032	0.010	MeV
E_f	100	100	100	100	MeV
B	185	565	180	610	G
A	10.5	9.0	9.5	8.2	arcsec
θ	27	20	22	29	degrees

δ corresponds to the electron index; N_e to the number density of the accelerated electrons with energy $E > E_0$; E_0 and E_f are the low and high energy cutoffs, respectively; B is the source magnetic field; A is the emitting area; and θ is the angle between the line of sight and the magnetic field direction.

these two scenarios; however, we have not been able to obtain them. In our fitting we considered the two scenarios and obtained two sets of source parameters. Results are shown in Table 1, where the parameters are those corresponding to gyrosynchrotron emission from homogeneous sources (Ramaty, 1969).

We do not see significant differences between the two models. Moreover, source sizes are of around 10 arcsecs. Looking at Figure 4 we observe that the distance between the reconnected arches is ∼30 arcsecs; that is, sources cannot overlap. Therefore, we reject Model 2 and consider the results of Model 1 only. The lower magnetic field intensity of source 1 is responsible for the low-frequency (∼10 GHz) peak in the spectrum, while the higher magnetic field intensity of source 2 produces a peak at around 15 GHz. Comparing with the magnetic field connectivity, we conclude that source 2 would correspond to the reconnected loops associated with the flare, while source 1 would correspond to the reconnected loops associated with the surge event. The optically thin part of source 1 is not observed because emission from source 2 prevails. Excellent fitting is observed in the optically thick regime, which is an indication that the simple homogeneous model is correct. The computed magnetic field intensities are consistent with the absolute values of the field obtained from the magnetic model for the corresponding set of reconnected loops. Viewing angles are of the order of 25 degrees; these values agree with those computed using the modeled magnetic field lines representing the reconnected loops; *i.e.*, from the model we can obtain the angle between the magnetic field vector and the line of sight. Source 1 has a harder electron distribution than source 2. However, its δ is not well determined since we do not observe the optically thin regime of sources.

The observed spectrum does not show evidence of suppression of emissivity at frequencies above 4 GHz. We then obtain an upper limit of the background plasma density in the source assuming that the Razin – Tsytovich frequency for mildly relativistic electrons (Dulk, 1985), $\nu_R[\mathrm{Hz}] = \nu_p^2/\nu_B \sim 29\, n[\mathrm{cm}^{-3}]/B[\mathrm{G}]$, is less than 1.2 GHz. The obtained upper limit for the background density N_{med} is 4×10^{10} cm^{-3}. Although most flares start with an impulsive phase, due to emission from accelerated particles followed by a gradual phase as the ambient medium reacts to the interaction with these particles, we have not observed a gradual phase in this event, even at submillimeter frequencies where it is more easily observed (see, *e.g.*, Trottet *et al.*, 2002, and Lüthi, Magun, and Miller, 2004). The plasma density derived here appears to be too low to produce significant thermal bremsstrahlung. If we consider 30 sfu as an upper limit for the density flux at 405 GHz and that at this frequency

the emission is optically thin, we obtain the following approximate formula for the expected flux density:

$$F_\nu(405\ \text{GHz}) \approx \frac{0.4 k_B}{c^2}\left(N_{\text{med}}^2 L \Omega\right)\frac{1}{\sqrt{T}} \tag{1}$$

where c is the speed of light, k_B is Boltzmann's constant, N_{med} is the plasma density in cm^{-3}, Ω and L are the size of the thermal source in arcseconds and its depth in centimeters, respectively, and T is the plasma temperature in Kelvins. Assuming typical values for $\Omega = 60$ arcsec and $L = 10^9$ cm, and substituting these values together with the previous N_{med} obtained in (1), we get a minimum value for the temperature of the thermal source $T \gtrsim 4.5 \times 10^6$ K.

5. Discussion and Conclusions

We presented a multi-wavelength, multi-technique analysis of a 1B/M6.9 flare that occurred on November 28, 2001, in AR 9715. The flare is followed by a surge. Though the dark chromospheric material is first seen in Hα images at ∼16:42 UT, by backward extrapolation taking into account the surge size and timing in two HASTA images (see Paper I), we can set its starting time at ∼16:34 UT, coincident with the flare maximum in Hα. The energy release that is responsible for flare activity is also capable of driving large amounts of cool (compared to coronal temperatures) material into the corona. Nevertheless, the physical mechanism involved in surges is only poorly understood. Two mechanisms have been proposed as surge drivers: a high pressure gradient in a magnetic tube (Steinolfson, Wu, and Schmahl, 1979) and magnetic energy release through reconnection (Heyvaerts, Priest, and Rust, 1977; Shibata, Nozawa, and Matsumoto, 1992; Kurokawa and Kawai, 1993; Schmieder *et al.*, 1996; Gaizauskas, 1996; Canfield *et al.*, 1996; Jibben and Canfield, 2004), in general, between newly emerging flux and the pre-existing surrounding field. Other possibilities involving magnetic reconnection (*e.g.*, at bald patches separatrices) have been also proposed (see Mandrini *et al.*, 2002).

In this particular event, the photospheric magnetic evolution (see Paper I) and the reconstructed magnetic topology lead us to conclude that magnetic reconnection was at the origin of the flare and surge. The reconnection process was driven by the emergence of two bipoles in the preexisting field in nearby sites. The bipole with the stronger field intensity (polarities 5 and 6 in Figure 1a) was first observed in an MDI image on November 27 at 16:03 UT (see Paper I). Computed magnetic field lines starting in this bipole interacted with the pre-existing field via reconnection, giving the flare Hα emission. The second bipole, which had a lower magnetic field intensity at the flare time (polarities 7 and 8 in Figure 1a), becomes visible almost one day before (see `mdi-evol-26-30nov.mpeg`). Field lines anchored in this bipole reconnected with the pre-existing magnetic configuration, and the set of reconnected large-scale field lines is parallel to the surge path (see Figure 4).

A double peak is observed in the radio spectrum during the maximum of the burst. We interpret this double peak as an indication of two emitting sources, in accordance also with the magnetic field evolution and computed topology. We worked out two models and showed that only Model 1, which assumes that sources do not overlap, is plausible. Therefore, the resulting electron beam parameters were obtained from the fitting to the observed radio spectrum of the added emission of two homogeneous gyrosynchrotron sources. This model implies that the particle injection should occur simultaneously within the time accuracy of OVSA data, which is 8 s. This is in agreement with the observed magnetic evolution

and deduced surge starting time. Furthermore, the parameters computed for the accelerated electron distributions producing the gyrosynchrotron emission (*i.e.*, B and θ) are in good agreement with those derived using the modeled magnetic field.

Acknowledgements We acknowledge the anonymous referee for very helpful comments and prompt answers. The authors thank the OVSA team and the SOHO/MDI and EIT consortia for their data. SOHO is a project of international cooperation of ESA and NASA. This study is partially based on data obtained at OAFA (El Leoncito, San Juan, Argentina) in the framework of the German – Argentinean HASTA/MICA Project, a collaboration of MPE, IAFE, OAFA, and MPAe. This research was partially supported by the Brazilian agency FAPESP (Contract No. 99/06126-7) and by the Argentinean grants UBACyT X329 (UBA), PICT 12187 (ANPCyT), and PIPs 6220 and 6266 (CONICET). C.H.M. and M.G.R. are members of the Carrera del Investigador Científico (CONICET). G.C. is a fellow of ANPCyT.

References

Alissandrakis, C.E.: 1981, *Astron. Astrophys.* **100**, 197.
Bastian, T.S., Benz, A.O., Gary, D.E.: 1998, *Annu. Rev. Astron. Astrophys.* **36**, 131.
Canfield, R.C., Reardon, K.P., Leka, K.D., Shibata, K., Yokoyama, T., Shimojo, M.: 1996, *Astrophys. J.* **464**, 1016.
Costa, J.E.R., Correia, E., Kaufmann, P., Magun, A., Herrmann, R.: 1995, *Solar Phys.* **159**, 157.
Costa, J.E.R., Silva, A.V.R., Lüdi, A., Magun, A.: 2002, *Astron. Astrophys.* **387**, 1153.
Cristiani, G., Martínez, G., Mandrini, C., Giménez de Castro, C., Rovira, M., Kaufmann, P., Levato, H.: 2005, *J. Atmos. Solar Terr. Phys.* **67**(17 – 18), 1744.
Delaboudinière, J.-P., Artzner, G.E., Brunaud, J., Gabriel, A.H., Hochedez, J.F., Millier, F., Song, X.Y., Au, B., Dere, K.P., Howard, R.A., Kreplin, R., Michels, D.J., Moses, J.D., Defise, J.M., Jamar, C., Rochus, P., Chauvineau, J.P., Marioge, J.P., Catura, R.C., Lemen, J.R., Shing, L., Stern, R.A., Gurman, J.B., Neupert, W.M., Maucherat, A., Clette, F., Cugnon, P., van Dessel, E.L.: 1995, *Solar Phys.* **162**, 291.
Démoulin, P., Bagala, L.G., Mandrini, C.H., Hénoux, J.C., Rovira, M.G.: 1997, *Astron. Astrophys.* **325**, 305.
Dulk, G.A.: 1985, *Annu. Rev. Astron. Astrophys.* **23**, 169.
Fernández Borda, R.A., Mininni, P.D., Mandrini, C.H., Gómez, D.O., Bauer, O.H., Rovira, M.G. 2002, *Solar Phys.* **206**, 347.
Gaizauskas, V.: 1996, *Solar Phys.* **169**, 357.
Green, L.M., López Fuentes, M.C., Mandrini, C.H., Démoulin, P., van Driel-Gesztelyi, L., Culhane, J.L.: 2002, *Solar Phys.* **208**, 43.
Heyvaerts, J., Priest, E.R., Rust, D.M.: 1977, *Astrophys. J.* **216**, 123.
Hurford, G.J., Read, R.B., Zirin, H.: 1984, *Solar Phys.* **94**, 413.
Jibben, P., Canfield, R.C.: 2004, *Astrophys. J.* **610**, 1129.
Kaufmann, P., Costa, J.E.R., Correia, E., Giménez de Castro, C.G., Raulin, J.-P., Silva, A.V.R.: 2000, Multiple high energy injections at the origin of solar flares. In: Ramaty, R., Mandzhavidze, N. (eds.) *High Energy Solar Physics Workshop — Anticipating Hessi, ASP Conf. Ser.* **206**, 318.
Klein, K.-L., Trottet, G., Magun, A.: 1986, *Solar Phys.* **104**, 243.
Kurokawa, H., Kawai, G.: 1993, In: Zirin, H., Ai, G., Wang, H. (eds.) *IAU Colloq. 141: The Magnetic and Velocity Fields of Solar Active Regions, ASP Conf. Ser.* **46**, 507.
Lüthi, T., Magun, A., Miller, M.: 2004, *Astron. Astrophys.* **415**, 1123.
Lee, J.W., Gary, D.E., Zirin, H.: 1994, *Solar Phys.* **152**, 409.
Mandrini, C.H., Démoulin, P., Schmieder, B., Deng, Y.Y., Rudawy, P.: 2002, *Astron. Astrophys.* **391**, 317.
Mandrini, C.H., Démoulin, P., van Driel-Gesztelyi, L., Schmieder, B., Cauzzi, G., Hofmann, A.: 1996, *Solar Phys.* **168**, 115.
Ramaty, R.: 1969, *Astrophys. J.* **158**, 753.
Ramaty, R., Schwartz, R.A., Enome, S., Nakajima, H.: 1994, *Astrophys. J.* **436**, 941.
Scherrer, P.H., Bogart, R.S., Bush, R.I., Hoeksema, J.T., Kosovichev, A.G., Schou, J., Rosenberg, W., Springer, L., Tarbell, T.D., Title, A., Wolfson, C.J., Zayer, I., MDI Engineering Team: 1995, *Solar Phys.* **162**, 129.
Schmieder, B., Rovira, M., Simnett, G.M., Fontenla, J.M., Tandberg-Hanssen, E.: 1996, *Astron. Astrophys.* **308**, 957.
Shibata, K., Nozawa, S., Matsumoto, R.: 1992, *Publ. Astron. Soc. Japan* **44**, 265.
Simões, P.J.A., Costa, J.E.R.: 2006, *Astron. Astrophys.* **453**, 729.
Steinolfson, R.S., Wu, S.T., Schmahl, E.J.: 1979, *Solar Phys.* **63**, 187.
Trottet, G., Raulin, J.P., Kaufmann, P., Siarkowski, M., Klein, K.-L., Gary, D.E.: 2002, *Astron. Astrophys.* **381**, 694.